01 Jan 1988

Characteristics and Optimal Design of Variable Airgap Linear Force Motors

Ming-Chuan Leu
Missouri University of Science and Technology, mleu@mst.edu

E. V. Scorza

D. L. Bartel

Recommended Citation

M. Leu et al., "Characteristics and Optimal Design of Variable Airgap Linear Force Motors," *Electric Power Applications*, Institute of Electrical and Electronics Engineers (IEEE), Jan 1988.
The definitive version is available at https://doi.org/10.1049/ip-b:19880037

Characteristics and optimal design of variable airgap linear force motors

M.C. Leu
E.V. Scorza
D.L. Bartel

Indexing terms: Linear motors, Power electronics, Optimisation, Computer application

Abstract: An analytical model for predicting the characteristics of variable airgap linear force motors is developed. The model takes into account magnetic losses, including the leakage and fringing effects, and the reluctance existing at the contacts between permanent magnets and polepieces. The model is validated by comparing its predicted characteristics with the results obtained from experiments and a finite element program. With the use of the modelled characteristics, computer programs based on the method of constrained steepest descent with state equations, is developed for automating and optimising the design of linear force motors. Numerical studies are made for both minimisation of weight and minimisation of power consumption.

List of symbols

A_a = cross-sectional area of constant airgap
A_g = cross-sectional area of working airgap
A_m = cross-sectional area of permanent magnet
AWG = American wire gauge
B_g = flux density in working airgap
B_m = flux density in permanent magnet
B_r = residual flux density of permanent magnet
D_0 = outside diameter of linear force motor
D_m = diameter of permanent magnet
F = force output from linear force motor
f = reluctance loss factor
f' = loss factor for leakage and fringing
G_f = force gain
H_{cm} = coercive force of permanent magnet
H_m = magnetic intensity of permanent magnet
I = current input
K_m = magnetic spring rate
L_a = length of constant airgap
L_g = length of working airgap with armature in central position
L_m = length of permanent magnet
L_0 = overall length of linear force motor
L_1 = coil section dimension in axial direction
L_2 = coil section dimension in radial direction
L_3 = length of polepiece section between permanent magnets
M = permanent magnet magnetomotive force
N = number of turns of coil windings
P = power consumption
R_a = reluctance of constant airgap
R_g = reluctance of working airgap
S = shape ratio (L_0/D_0)
t = thickness
U = perimeter of cross-section of working airgap
$\boldsymbol{u}$ = design variables
W = weight
X = armature position ($X = 0$ represents the central position)
$\boldsymbol{x}$ = state variables
α = parameter associated with loss factor
μ_m = permeability of permanent magnet
μ_0 = permeability of free space
ρ = coil resistivity
ρ_p = density of polepiece and armature
ρ_m = density of permanent magnet
ρ_c = density of coil material
σ = parameter associated with loss factor
ϕ = magnetic flux

Paper 6276B (P1/S8) first received 28th October 1987 and in revised form 17th June 1988

M.C. Leu is with the Department of Mechanical Engineering, New Jersey Institute of Technology, Newark, New Jersey, U.S.A.

E.V. Scorza is with the Department of Mechanical Engineering, University of Costa Rica, San Jose, Costa Rica

D.L. Bartel is with the Sibley School of Mechanical and Aerospace Engineering, Cornell University, Ithaca, New York, U.S.A.

1 Introduction

A variable airgap linear force motor is an electromagnetic device which creates a force from an electric input current. The current input generates magnetic control flux which interacts with the polarising flux generated at the working airgaps by the permanent magnets, thus creating a force on the armature. The armature is movable in the working airgaps. The movement of the armature is in contrast to the movement of the coil in other electromagnetic devices such as loudspeakers and vibration shakers. For this reason, the linear force motor is called a moving-iron actuator, instead of a moving-coil actuator [1]. The device is used in many applications, including latching and servo-actuation.

With the discovery of rare earth magnetic materials such as samarium–cobalt based permanent magnets [2], the performance of linear force motors has been greatly increased in the recent past. The samarium–cobalt material can be magnetised to higher flux density levels, and it has greater resistance to demagnetisation. The availability of this new magnetic material, however, also calls for a new design approach in order to maximise performance improvement without tedious and costly cut-

and-try experimentation. This critical need motivated this study.

The study of linear force motor design presented in this paper started with modelling the characteristics of the device. The design problem was then formulated as a mathematical optimisation problem. A computer optimisation program based on the method of steepest descent with state equations [3], which is capable of generating a set of design parameters that satisfy a specified performance index and minimise either weight or power consumption, was developed.

2 Modeling of motor characteristics

A schematic diagram of linear force motor is shown in Fig. 1. The device has a rotational symmetry about its axis of action. There are two cylindrically shaped permanent magnets in contact with the polepieces. The movable armature is in the form of a circular ring. The polepieces channel the flux generated by the permanent magnets from the ends of the magnets to the airgaps. There are two types of airgap: one is a fixed airgap which has a constant gap length, and the other is a working airgap which has a variable gap length. An input current to the coil creates a magnetic control flux which interacts with the flux generated by the permanent magnets at the working airgaps, thus creating a force on the armature. Reversing the polarity of the input current reverses the direction of the control flux across the working airgap, thereby reversing the direction of the force on the armature. When the control flux is not equal to zero, the flux balance produced by the two permanent magnets is upset, and the armature moves in the direction of the net flux.

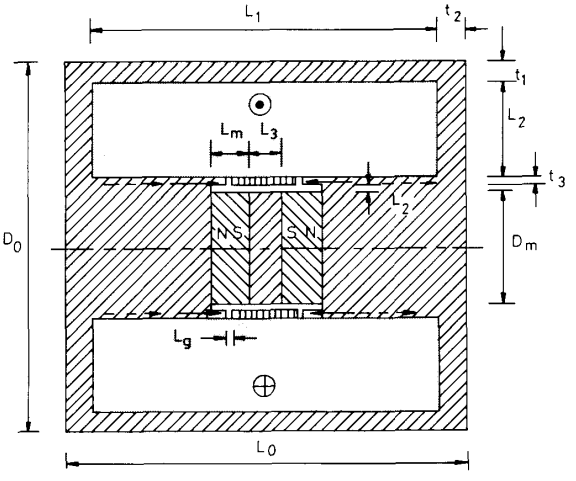

Fig. 1 *Schematic representation of linear force motor*
▨ polepiece ▧ permanent magnet
▥ armature □ coil windings
→ directions of permanent magnent fluxes
--→ direction of control flux for an assumed input current polarity (⊙ and ⊕)

By using an equivalent magnetic circuit technique, an analytical model for studying the characteristics of the linear force motor was established. The equivalent circuit for the device is shown in Fig. 2, which consists of (*a*) the reluctances R_1 and R_2 which are associated with the working airgaps, and R_a which is associated with the constant airgap; (*b*) the magnetic sources M_1 and M_2 which are associated with the permanent magnets, and NI which is associated with the coil turns and the current input; and (*c*) the 'effective' (i.e. with magnetic losses taken into consideration) fluxes ϕ_1, ϕ_2, and ϕ_3 passing

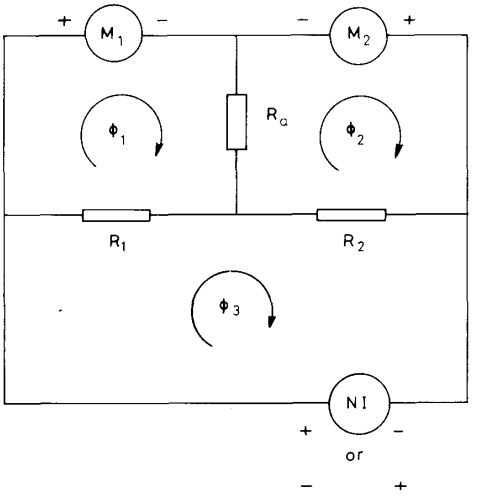

Fig. 2 *Equivalent magnetic circuit for linear force motor*

through the magnetic source fields. The reluctances due to the polepieces and the armature were neglected because the permeability of the soft-iron material is three orders of magnitude larger than the permeability of air [4, 5].

Applying the equivalent Kirchhoff's voltage law to each of the three magnetic loops in Fig. 2 yields

$$\begin{bmatrix} (R_1 + R_a) & -R_a & -R_1 \\ -R_a & (R_2 + R_a) & -R_2 \\ -R_1 & -R_2 & (R_1 + R_2) \end{bmatrix} \times \begin{bmatrix} \phi_1 \\ \phi_2 \\ \phi_3 \end{bmatrix} = \begin{bmatrix} -M_1 \\ M_2 \\ NI \end{bmatrix} \quad (1)$$

where the reluctances are

$$R_1 = \frac{L_g + X}{\mu_0 A_g} \quad (2)$$

$$R_2 = \frac{L_g - X}{\mu_0 A_g} \quad (3)$$

$$R_a = \frac{L_a}{\mu_0 A_a} \quad (4)$$

For the samarium–cobalt permanent magnet, the B/H relationship in the second quadrant is linear as shown in Fig. 3. Thus:

$$H_m = H_{cm} + \frac{B_m}{\mu_m} = \frac{B_m - B_r}{\mu_m} \quad (5)$$

The flux densities in the two permanent magnets can be expressed as follows:

$$B_{m1} = \frac{-\phi'_1}{A_m} \quad (6)$$

$$B_{m2} = \frac{\phi'_2}{A_m} \quad (7)$$

The 'prime' symbol is imposed to acknowledge the fact that the magnetic flux leaving the permanent magnet reduces its magnitude when it reaches the airgap, owing

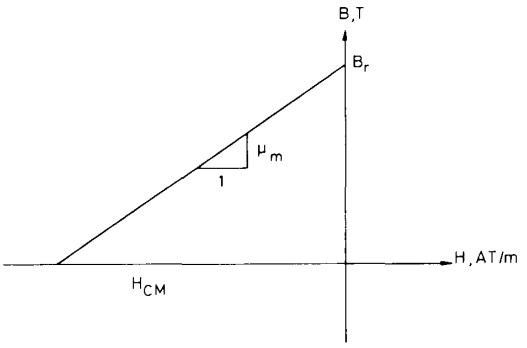

Fig. 3 *Second quadrant of B/H plane of samarium–cobalt permanent magnet*

$H_{CM} = 7.3232 \times 10^5$ $B_r = 0.94$

to the existence of leakage and fringing losses [6]. These losses can be accounted for by introducing a loss factor f', defined as

$$f'_1 = \frac{\phi'_1}{\phi_1} \quad \text{and} \quad f'_2 = \frac{\phi'_2}{\phi_2} \tag{8}$$

In addition to leakage and fringing effects, the contacts between the permanent magnets and the polepieces create reluctances at the joints which can be included by using a reluctance factor f defined as

$$f = \frac{-H_m L_m}{M} \tag{9}$$

By substituting eqns. 6–9 into eqn. 5, the magnetomotive forces of the permanent magnets can be expressed as

$$M_1 = \frac{f'_1 \phi_1 L_m}{f \mu_m A_m} - \frac{H_{cm} L_m}{f} \tag{10}$$

$$M_2 = -\frac{f'_2 \phi_2 L_m}{f \mu_m A_m} - \frac{H_{cm} L_m}{f} \tag{11}$$

Substituting the above two equations into eqn. 1 yields

$$\begin{bmatrix} \left(R_1 + R_a + \dfrac{f'_1 L_m}{f \mu_m A_m}\right) & -R_a & -R_1 \\ -R_a & \left(R_2 + R_a + \dfrac{f'_2 L_m}{f \mu_m A_m}\right) & -R_2 \\ -R_1 & -R_2 & (R_1 + R_2) \end{bmatrix} \times \begin{bmatrix} \phi_1 \\ \phi_2 \\ \phi_3 \end{bmatrix} = \begin{bmatrix} \dfrac{H_{cm} L_m}{f} \\ -\dfrac{H_{cm} L_m}{f} \\ NI \end{bmatrix} \tag{12}$$

Values of the reluctance loss factor f are usually between 1.0 and 1.5, depending upon the condition of contact between permanent magnets and polepieces; values of f', however, vary widely and often cannot be determined with a high degree of accuracy [1]. Empirical equations have been developed by several researchers [5, 6, 7] to estimate the values of f' for magnetic devices of various configurations. Nevertheless, those devices have geometries significantly different from the one being studied, and thus the empirical equations were not directly applicable to this study. A technique for estimating f' is to construct a magnetic field plot by sketching the flux distribution and equipotential lines of the entire magnetic field [5]. This may be done most effectively by incorporating finite element methods.

The approach utilised in this study for estimating f' was to propose a relationship taking into account the lengths and cross-sectional areas of the airgaps plus the armature displacement. The relationship is a modification of the formulae presented in Reference 6 and 7 for devices with similar geometric features, and is

$$f' = 1 + \left(\frac{L_g \pm \alpha X}{A_g} + \frac{L_a}{A_a}\right)\sigma U \tag{13}$$

where the two parameters σ and α can be determined from, for example, plotting of flux field or experimental measurement. In this study, values of σ and α were chosen so that the flux densities in the airgaps predicted by the analytical model can best match that obtained from a finite element program. The comparison will be given in the next Section.

Eqn. 12 can be easily solved to obtain ϕ_1, ϕ_2, and ϕ_3. The flux in the working airgaps can then be calculated as

$$\phi_{g1} = \phi_1 - \phi_3 \tag{14}$$

$$\phi_{g2} = \phi_2 - \phi_3 \tag{15}$$

The force output can then be computed using the following equation

$$F = \frac{\phi_{g1}^2 - \phi_{g2}^2}{2\mu_0 A_g} \tag{16}$$

From the forces computed for different armature displacements and input currents, the magnetic spring rate ($\partial F/\partial X$) and the force gain ($\partial F/\partial I$) can be computed.

3 Comparison of analytical results with FEM and experimental results

The analytical model presented in the previous section was verified by comparing its predicted values of motor characteristics with the results obtained from a finite element program and from experimental measurement. Table 1 shows a comparison of the values predicted by the model with those obtained from the finite element program AOS/MAGNETIC [8]. The actual data have been nondimensionalised for ease of comparison. In the predicted characteristics, the values of f, σ and α were determined so as to provide the best match between the results of the analytical model and those obtained from the finite element program. Despite the simplicity of the

Table 1: Comparison between results of analytical model and that of AOS/MAGNETIC program

			AOS/MAGNETIC			Analytical model		
L_g	X	I	B_{g1}	B_{g2}	F	B_{g1}	B_{g2}	F
0.83	0	0	−1.00	1.00	0	−1.00	1.00	0
0.92	0	0	−9.97	0.97	0	−0.97	0.97	0
1.00	0	0	−0.94	0.94	0	−0.94	0.94	0
1.00	0.33	0	−0.66	1.31	0.21	−0.67	1.32	0.21
1.00	0.38	0	−0.63	1.36	0.24	−0.64	1.38	0.24
1.00	0.42	0	−0.60	1.43	0.28	−0.60	1.43	0.28
1.00	0.42	1.0	0.20	2.47	1.00	0.28	2.44	0.97
1.00	0.42	−1.0	−1.43	0.27	0.33	−1.40	0.31	0.31

analytical model, Table 1 shows that an excellent agreement has been achieved.

The predicted characteristics were also compared with experimental results. Fig. 4 shows the force-current-displacement relationship of the device for a typical working

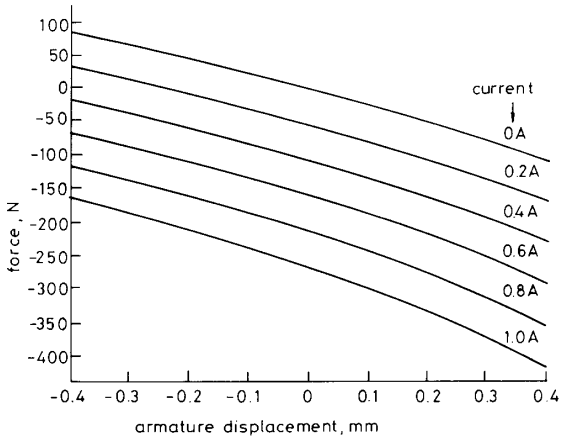

Fig. 4 *Force-current-displacement relationship of linear force motor*

airgap length using the analytical model. From this relationship, the magnetic spring rate and the force gain were computed. The values of these parameters and the predicted flux density were compared with those measured experimentally. The comparisons are:

(*a*) magnetic spring rate (with zero current input)

$\partial F/\partial X$ (measured) = 236 N/mm

$\partial F/\partial X$ (predicted) = 227 N/mm

(*b*) force gain (at central plunger position)

$\partial F/\partial I$ (measured) = 289 N/A

$\partial F/\partial I$ (predicted) = 268 N/A

(*c*) flux density in working airgap (with zero current input and at central plunger position)

B_g (measured) = 0.680 T

B_g (predicted) = 0.655 T

The above comparisons show a good agreement between the predicted and the measured characteristics. It should be noted that a closer agreement with the measured results could have been obtained if values for the loss factors in the analytical model had been selected to match the measured results, instead of matching the finite element results as was done.

4 Optimal design problem formulation

An optimal design problem may be formulated as follows: choose $\boldsymbol{u}$ to minimise $f_0(\boldsymbol{x}, \boldsymbol{u})$, subject to $\boldsymbol{h}(\boldsymbol{x}, \boldsymbol{u}) = 0$, and $\boldsymbol{\phi}(\boldsymbol{x}, \boldsymbol{u}) \leqslant 0$. $\boldsymbol{u}$ is the vector of design variables, $\boldsymbol{x}$ is the vector of state variables, f_0 is the objective function, $\boldsymbol{h}$ represents equality constraint functions, and $\boldsymbol{\phi}$ represents inequality constraint functions.

For the device studied, the design and state variables were (refer to Fig. 1)

$$\boldsymbol{u} = [L_m, D_m, L_g, t_3, L_a, \text{AWG}, L_1, L_2]$$

$$\boldsymbol{x} = [N, L_3, t_1, t_2, L_0, D_0]$$

4.1 Objective functions

Two objective functions were considered: weight and power consumption. The weight of the device is the summation of the weights of polepieces, coils, armature, and permanent magnets. It can be expressed as

$$W = \rho_p \pi\{L_0 D_0^2/4 - 2L_g t_3(D_m + 2L_a + t_3) - L_1 L_2(D_0 - 2t_1 - L_2)\} + (\rho_m - \rho_p)(\pi/2)L_m D_m^2 + \rho_c \pi(D_w^2/4)N(D_m + 2L_a + 2t_3 + L_2) \quad (17)$$

The power consumption is essentially the rate of heat generated due to the coil resistance. It relates to coil current and coil resistance simply as $P = I^2R$, which can be expressed in terms of design and state variables as

$$P = 4I^2\rho(2L_a + 2t_3 + D_m + L_2)N/D_w^2 \quad (18)$$

4.2 Equality constraints

The equality constraints arise from the relationships among the variables which represent the dimensions of the device. First, the number of coil turns depends upon the coil wire diameter and the space available for the coils. This relationship can be expressed as*

$$N = \text{integer}\left[\frac{L_1 L_2 10^{(c_5 + c_6 \text{AWG})}}{\{D_w 10^{(c_3 + c_4 \text{AWG})}\}^2 + 0.5}\right] \quad (19)$$

where

$$D_w = 10^{(c_1 + c_2 \text{AWG})/2} + 0.5 \times 10^{-4}$$

The exponents c_i, $i = 1 - 6$, are empirical constants.

Second, the capacity of the polepiece in channeling magnetic flux is limited by its minimum cross-sectional area. To save material, the cross-sectional area of the polepiece should be kept constant at critical locations. This imposes the following relationships:

$$L_3 = \frac{2t_3(D_m + 2L_a + t_3)}{2D_m} \quad (20)$$

$$t_1 = \frac{-(D_m + 2(L_a + t_3 + L_2)) + [(D_m + 2(L_a + t_3 + L_2))^2 + 4t_3(D_m + 2L_a + t_3)]^{1/2}}{2} \quad (21)$$

$$t_2 = \frac{t_3(D_m + 2L_a + t_3)}{(D_m + 2L_a + 2t_3 + L_2)} \quad (22)$$

Finally, the variables as designated (Fig. 1) must satisfy the following geometric relationships:

$$L_0 = L_1 + 2t_2 \quad (23)$$

$$D_0 = D_m + 2(L_a + t_3 + L_2 + t_1) \quad (24)$$

4.3 Inequality constraints

There are two types of inequality constraints: one associated with performance requirements and the other associated with geometric dimensions. First, the values of magnetic spring rate K_m ($=\partial F/\partial X$), force gain G_f ($=\partial F/\partial I$), and shape factor S ($=L_0/D_0$) should lie within desired ranges, i.e.

$$K_{m,min} \leqslant K_m \leqslant K_{m,max}$$
$$G_{f,min} \leqslant G_f \leqslant G_{f,max} \quad (25)$$
$$S_{min} \leqslant S \leqslant S_{max}$$

* Private communication with Hans Toews of Moog Inc., East Aurora, New York, U.S.A.

Second, the geometry of the device naturally imposes the following constraints:

$$L_g \leqslant L_m \tag{26}$$

$$2L_m + L_3 \leqslant L_1 \tag{27}$$

Finally, the values of the design variables should not exceed specified upper and lower bounds, i.e.

$$\begin{aligned}
&L_{m,\,min} \leqslant L_m \leqslant L_{m,\,max}\\
&D_{m,\,min} \leqslant D_m \leqslant D_{m,\,max}\\
&L_{g,\,min} \leqslant L_g \leqslant L_{g,\,max}\\
&t_{3,\,min} \leqslant t_3 \leqslant t_{3,\,max}\\
&L_{a,\,min} \leqslant L_a \leqslant L_{a,\,max}\\
&\mathrm{AWG}_{min} \leqslant \mathrm{AWG} \leqslant \mathrm{AWG}_{max}\\
&L_{1,\,min} \leqslant L_1 \leqslant L_{1,\,max}\\
&L_{2,\,min} \leqslant L_2 \leqslant L_{2,\,max}
\end{aligned} \tag{28}$$

5 Results of optimal design study

The method of constrained steepest descent with state equations [3] was used as the basis for developing a computer program for the optimal design study. Starting with an initial estimate of the design, this method determines a set of design parameters which optimises an objective function and satisfies equality and inequality constraints. In this study, the initial estimates for the design variables were the parameter values obtained from actual device units.

The optimisation process involves many iterations. In each iteration, the optimisation algorithm computes a small change in values of the design variables so as to reduce the objective function and simultaneously direct the solution search toward the feasible region. This computation involves the checking of violation against inequality constraints, and computing the gradients of objective and equality constraint functions with respect to design and state variables. The iteration process continues until a stopping criterion has been met. Particularly worth noting in the computation is the procedure of determining whether K_m and G_f are within constrained ranges. To do this, first the values of design and state variables are used in eqns. 2–4 to compute reluctances, then in eqns. 12–15 to compute fluxes, and finally in eqn. 16 to compute forces. K_m and G_f are then obtained by varying armature positions and input currents, also using this set of equations.

The results of the optimisation study are summarized in Table 2, where the actual data have been nondimensionalised with respect to the values of the parameters in the existing design. The Table shows that the unit being studied can be reduced by 30% in weight or by 45% in power consumption, with the performance characteristics represented by K_m, G_f and S remaining unchanged.

In addition to being able to minimise weight or power consumption while keeping the same performance characteristics, the optimisation program can also be used to design units of the device with different performance characteristics from the existing units. This is also illustrated in Table 2 which shows that the values of K_m, G_f and S can be varied.

Table 2: Summary of design optimisation study

	Initial design	Optimal design						
		minimisation of weight			minimisation of power			
		Test number			Test number			
		1	2	3	1	2	3	4
K_m	1.00	1.00	0.46	1.00	1.00	2.30	1.00	1.00
G_f	1.00	1.00	1.00	1.00	1.00	1.00	1.84	1.00
S	1.00	1.00	1.00	1.47	1.00	1.00	1.00	0.66
W	1.00	0.70	0.86	1.00	1.29	1.30	2.11	1.53
P	1.00	1.37	2.06	1.51	0.55	0.43	1.11	0.70

6 Conclusions

An analytical model describing the characteristics of linear force motors has been developed. The model is capable of predicting the force-current-displacement relationship, and other motor characteristics. The predicted characteristics agree well with both experimental and finite element results.

A computer program based on an optimisation algorithm has been developed for automating and optimising the motor design. The program is capable of generating an optimal set of design parameters for minimising weight or power consumption, while satisfying specified performance characteristics.

7 Acknowledgments

The financial support of this study was provided by Moog Inc. We thank R.A. Aubrecht and D.H. Morash for being instrumental in initiating this project, and for providing advice and encouragement during the course of the work.

8 References

1 EZEKIEL, F.D.: 'Electromagnetic actuators', *Inst. and Control Syst.*, **40**, (12), 1967, pp. 90–96
2 PARKER, R.J.: 'Rare-earth permanent magnets move into new applications', *Electronics*, 1974, **47**, (25), pp. 119–123
3 HAUG, E.J., and AURORA, J.S.: 'Applied optimal design' (Wiley-Interscience, New York, 1979)
4 MOON, F.C.: 'Magneto-solid mechanics' (John Wiley & Sons, New York, 1984)
5 ROTERS, H.C.: 'Electromagnetic devices' (Chapman and Hall, Ltd., London, 1945)
6 McCAIG, M.: 'Permanent magnets in theory and practice' (Billings & Sons, Ltd., London, 1977)
7 HADFIELD, D.: 'Permanent magnets and magnetism' (John Wiley & Sons, Inc., New York, 1962)
8 AOS/MAGNETIC is a product of A.O. Smith Data Systems Inc., 8901 N. Kildeer Court, Milwaukee, Wisconsin, U.S.A.